Contents lists available at ScienceDirect

Food and Bioproducts Processing

journal homepage: www.elsevier.com/locate/fbp

The effect of spray-drying inlet conditions on iron encapsulation using hydrolysed glucomannan as a matrix

*Dyah Hesti Wardhani**, *Irsyadia Nindya Wardana*, *Hana Nikma Ulya*, *Heri Cahyono*, *Andri Cahyo Kumoro*, *Nita Aryanti*

Department of Chemical Engineering, Faculty of Engineering, Diponegoro University, Jl. Prof. Soedarto, SH, Semarang, Central Java, Indonesia 50275

ARTICLE INFO

Article history:
Received 13 October 2019
Received in revised form 17 April 2020
Accepted 29 May 2020
Available online 10 June 2020

Keywords:
Glucomannan encapsulant
Hydrocolloid
Hydrolised glucomannan
Iron encapsulation
Spray-drying

ABSTRACT

Spray-drying is an encapsulation method that can be used to protect iron from oxidation. Hydrolysed glucomannan has shown potential as an encapsulant due to its ability to form a fine, dense network upon drying. The aim of this study was to evaluate the potential of hydrolysed glucomannan as a matrix for iron at inlet air temperatures of spray-drying of 110 °C, 120 °C, 130 °C and 140 °C. The physicochemical properties and performance of the iron encapsulation powder were determined. The results indicated that the inlet air temperature influences the properties and performance of the powder. An increase in the inlet air temperature from 110 °C to 140 °C led to a greater loading capacity and particle size distribution but had an insignificant impact on the moisture content, solubility and swelling. Higher drying air temperatures tended to produce a darker powder. The morphological analysis revealed that higher inlet drying air temperatures produced powders with rounder shapes, whereas lower temperatures produced irregular shapes that tended to form deep concavities on the powder surface. The samples from all inlet temperatures showed similar functional groups but in different intensities. The release of iron at pH 6.8 was higher for the lower inlet temperatures. Samples with the highest inlet temperature showed the highest performance in protecting iron from oxidation. Considering the performance, 130 °C is recommended as the inlet air temperature for iron spray-drying encapsulation using hydrolysed glucomannan.

1. Introduction

Iron is used in the process of oxygen absorption in the blood, which is ultimately used in digesting food for the process of physical growth and development (Gupta, 2014). Iron requirements are influenced by many factors, including gender and age. Iron deficiency or anaemia occurs commonly in infants and pregnant women. Although rarely resulting in death, iron deficiency can still impair cognitive performance and immune system function at all stages of life. Moreover, it affects work capacity and productivity (WHO, 2001).

Since a limited degree of iron content is found in dietary products, the intake of iron could be fulfilled by taking iron supplements or consuming fortified foods (Bryszewska, 2019). However, individual choices can substantially alter dietary components, changing the solubility and absorption of the iron (Hunt, 2003). Encapsulation could help defend against iron deterioration. This approach can also protect iron from oxidation, which can lead to unpleasant odours, tastes and appearances. In addition, it shields the iron from interactions with inhibitors that reduce its bioavailability due to chelation (Bryszewska, 2019).

Currently, spray-drying, in which a solution of a selected compound is converted into a dry powder, is one of the most popular encapsulation techniques. This process works by removing the solvent of a dispersion of the desired com-

* Corresponding author.
E-mail address: dhwardhani@che.undip.ac.id (D.H. Wardhani).
https://doi.org/10.1016/j.fbp.2020.05.013

pound in a matrix solution through atomization in hot air, resulting in a powder (Jana et al., 2017). The matrix used as an encapsulating material must be food-grade, biodegradable and able to form a barrier between the internal element and its surroundings (Nedovic et al., 2011). The neutral polysaccharide glucomannan fulfils these requirements for use as an encapsulation matrix. Beyond good film formation, a high level of water solubility and edibility, glucomannan is able to form a fine, dense network upon drying (Wattanaprasert et al., 2017). However, its high viscosity, which measures more than 4000 cps for a 1% solution of 73% purity glucomannan (Wardhani et al., 2015), places limitations on the application of glucomannan in spray-drying encapsulation. Given that the highest possible viscosity for a typical spray dryer is only 300 cps, the high viscosity of glucomannan can cause blockage of the nozzle of the spray dryer (Sosnik and Seremeta, 2015). However, Wattanaprasert et al. (2017) reported that 1500 units of mannanase are able to hydrolyse and reduce 18% glucomannan to a viscosity of 285 cps. Cellulase, which is a mixture of endoglucanase, exoglucanase and glucosidase, is the most common enzyme used for glucomannan hydrolysis (Jiang et al., 2018). Hydrolysed glucomannan has been used to encapsulate various active compounds, such as andrographolide (Wattanaprasert et al., 2017) and antitubercular drugs (Guerreiro et al., 2019).

Prior research on iron encapsulation using the spray-drying method has been carried out by Churio and Valenzuela (2018) and Romita et al. (2011). The former (Churio and Valenzuela, 2018) reported various concentrations of bovine erythrocytes and ferrous sulphate using 40% maltodextrin. Meanwhile, Romita et al. (2011) used carboxymethyl cellulose, gum arabic and different ratios of hydroxypropylmethyl cellulose and maltodextrin as an encapsulation matrix for ferrous fumarate. Neither report, however, studied the effects of the spray-drying conditions on the resultant powder properties. In contrast, other investigations, including the studies by Santhalakshmy et al. (2015), Shi et al. (2018), and Tran and Nguyen (2018), have reported on the impacts of spray-drying conditions on the resultant powder properties. Still, the evaluation of the impact of inlet spray-drying temperature on iron encapsulation using hydrolysed glucomannan has not yet been explored. Therefore, the aim of the present study was to evaluate the effects of the inlet drying air temperature on the performance of iron encapsulation using hydrolysed glucomannan prepared by the spray-drying method. This paper presents novel observations of the efficacy of enzymatically hydrolysed glucomannan as an iron encapsulant using the spray-drying method.

2. Materials and methods

2.1. Materials

This work used glucomannan (100%, Now Foods, Bloomingdale, IL, USA), *Aspergillus niger* cellulase (Sigma–Aldrich, St. Louis, MO, USA, C1184, powder, activity ≥0.3 units/mg solid), iron(II) sulphate heptahydrate ($FeSO_4{\cdot}7H_2O$, Merck, Kenilworth, NJ, USA) and other pro analyst quality compounds.

2.2. Glucomannan hydrolysis and iron loading

A 100-mL glucomannan solution (2%, w/v) was prepared in distilled water at 3000 rpm homogenisation (RW 16 basic; IKA-Werke, Staufen im Breisgau-German). After the glucomannan was completely dissolved, cellulase was added to obtain a final concentration of 20 ppm under 3000 rpm homogenisation for 12 h at 30 °C. Next, the solution was boiled for 10 min to deactivate the enzyme. After the solution reached room temperature, 0.375 g of $FeSO_4{\cdot}7H_2O$ was dissolved in it.

2.3. Iron encapsulation via the spray-drying method

Spray-drying experiments were carried out using a Mini Spray Dryer B-290 (BÜCHI Labortechnik AG, Flawil, Switzerland). The spraying system included a two-fluid nozzle composed of an internal tip with an opening measuring 0.7 mm in diameter. The dry air flow rate, liquid feeder pump flow and aspiration of the spray dryer were set to 667 L/h, 0.18 L/h and 90%, respectively, for all experiments. The hydrolysed product solution was sprayed at various inlet drying air temperatures (110 °C, 120 °C, 130 °C and 140 °C).

2.4. Moisture content

The encapsulated iron powder was examined to determine its moisture content following the Association of Official Agricultural Chemists' method at 105 °C until the sample weight was steady (AOAC, 2000).

2.5. Iron content and loading capacity

The iron content of the encapsulated sample was determined based on the method of Veerabhadraswamy et al. (2018), with slight modifications, using a visible spectrophotometer (B-One, 50 DA-X). The encapsulated sample (0.2 g) was dissolved in 20 mL of distilled water. Ten millilitres of this solution were placed in a 100-mL flask and reacted with 10 mL of phenanthroline (1 g/L), 8 mL of sodium acetate solution (1.2 M) and 1.0 mL of hydroxylamine solution (100 g/L). Distilled water was used to fill the flask up to 100 mL. After 10 min of colour development, the absorbance of the samples was read at a wavelength of 510 nm. Loading capacity (LC) was calculated following Guerreiro et al. (2019). The LC was described as ratio between the mass of iron in the spray-dried product and the mass of spray-dried powder as follows:

$$\text{LC} \quad (\%) = \frac{m_{iron}\,(\text{mg})}{m_{powder}\,(\text{mg})} \times 100\% \tag{1}$$

2.6. Solubility and swelling

The solubility and swelling of the powder particles were measured following the method of Wardhani et al. (2019a). Ten millilitres of solution were prepared by diluting 0.1 g of the sample, and the solution was subsequently heated in a water bath at 60 °C for 30 min. The supernatant was then separated using centrifugation at 4000 rpm for 10 min. The supernatant was collected prior to oven drying. The weights of the wet and dried supernatant were recorded for solubility determination. Meanwhile, the weight of the wet and dried paste was also recorded after separation for swelling determination:

$$\text{Solubility}\,(\%) = \frac{\text{weight of dried precipitate}}{\text{weight of supernatant}} \times 100\% \tag{2}$$

$$\text{Swelling} = \frac{\text{weight of paste}}{\text{weight of dried paste}} \tag{3}$$

2.7. Particle size distribution

The particle size distribution was determined using a particle size analyser (Malvern Panalytical, Malvern, UK) at 25 ± 1.0 °C with a duration of 50 s, a measurement position of 3.00 mm, and an attenuator level of 8, with water as the dispersant.

2.8. Colour

The colour analysis of the particle product was performed using the Chroma Meter (CR-300; Minolta Co., Ltd., Osaka, Japan). The L^*, a^* and b^* values of the samples were determined. L^* represents the lightness of the samples in the direction of darkness to lightness (0 = black, 100 = white), while a^* corresponds to the scale of green (−60) to red (60), with negative values for greenness and positive values for redness (−120 to 120). Lastly, b^* presents negative values for blueness (−60) and positive values for yellowness (60) (Rigon and Noreña, 2016). The colour difference (ΔE) was calculated as below:

$$\Delta E = \sqrt{(L_o^* - L^*)^2 + (a_o^* - a^*)^2 + (b_o^* - b^*)^2} \quad (4)$$

The colour values of the native glucomannan powder (L_o^*, a_o^* and b_o^*) were used as references in determining the colour difference.

2.9. Morphology of the particle surface and functional groups

An analysis of the functional groups in the sample was carried out using Fourier-transform infrared spectroscopy (FT-IR) (PerkinElmer Frontier™; PerkinElmer, Waltham, MA, USA). The particle morphology and the quantity of iron on the particles' surfaces were determined using scanning electron microscopy (JSM-6510 LV JEOL Ltd., Tokyo, Japan) at 20 kV with a magnification of 3000×, equipped by energy dispersive X-ray (EDX)-spot scanner.

2.10. Iron release profile

The release profile of iron was observed in a pH 6.8 phosphate buffer (0.1 M) solution by placing 0.1 g of the sample in an Erlenmeyer flask with 50 mL of the buffer solution. After shaking for a certain amount of time, the filtrate was collected and examined for released iron.

2.11. Storage stability

The iron stability was evaluated with respect to the efficacy of the encapsulation in preventing iron oxidation. The powders (0.2 g) were placed in an uncovered porcelain dish stored at ambient temperature (28.0 ± 1.6 °C). The evaluation of iron oxidation was conducted at 120 days by diluting the powder in distilled water (20 mL) and measuring the iron content:

$$\text{Iron retention} \quad (\%) = \frac{\text{iron}_{t=120\,\text{day}}}{\text{iron}_{t=0\,\text{day}}} \times 100\% \quad (5)$$

2.12. Statistical analysis

All the data were performed in triplicate for each condition and were expressed as mean ± standard deviation. A one-way analysis of variance (ANOVA) was performed to compare the groups. This statistical analysis was run using Ms. Excel 2019. Differences in the data were considered to be significant at a level of $p < 0.05$.

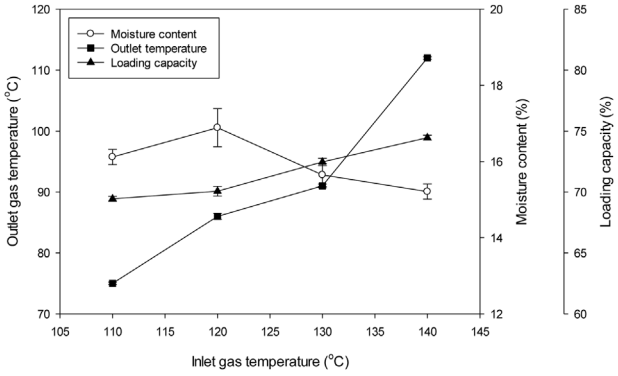

Fig. 1 – Outlet temperature, moisture content and loading capacity of encapsulated iron at various inlet spray-drying gas temperatures ($p < 0.05$).

3. Results and discussion

3.1. Outlet temperature and moisture content

The outlet gas temperature, moisture content and loading capacity of the encapsulated iron at different drying inlet air temperatures are presented in Fig. 1. An increase in the inlet gas temperature in spray-drying promotes a rise in the outlet gas temperature and a decrease in the water content of the encapsulated sample. In this study, the outlet temperatures were lower than the inlet ones since the energy carried by the inlet gas was transferred to the liquid feed of the spray dryer, which has a lower temperature during the drying process ($p < 0.05$). Moreover, our results showed a tendency for higher inlet drying air temperatures to promote a lower moisture content ($p < 0.05$). Similar results have been obtained by other authors, including Avila et al. (2015), Dantas et al. (2018), Mishra et al. (2014) and Moghaddam et al. (2017). The temperature of the drying air inlet during spray-drying had effects on the temperature of the gas output, particle size, yield and water content (Arpagaus et al., 2017). Increasing the gas inlet temperature induced a drying rate that provoked an increase in the evaporation of water. As a result, the higher inlet temperatures tended to have lower moisture contents than the lower temperatures. Although the total difference in the moisture content over the range of gas inlet temperatures tested (110–140 °C) was just above 1%, the moisture content of each inlet temperature was significantly different ($p < 0.05$). This result suggests that the differences between the gas inlet and outlet temperatures were smaller at the highest gas inlet temperature than at the lower gas inlet temperatures. This could be due to an instant crust formation on the surface of the particles at the highest temperatures, making it difficult for water to diffuse across the particle surface (Tontul and Topuz, 2017). This result is supported by the particle morphology analysis, which showed a fast drying rate at high temperatures. Hence, these particles tended to have larger sizes because of the formation of instant crust layers on the surface (Fig. 4).

3.2. Loading capacity

Loading capacity was described as the amount of iron actually in the microcapsule compared to the total amount of powder.

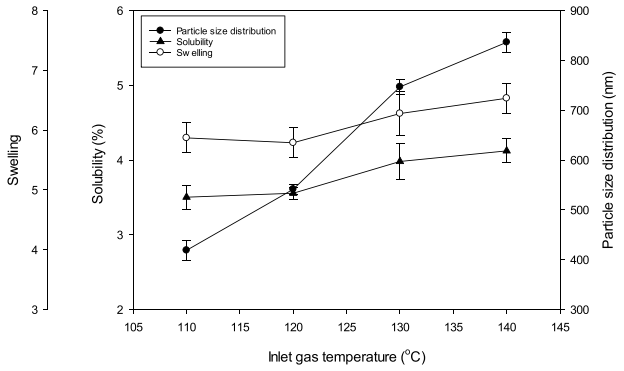

Fig. 2 – Swelling, solubility and particle size distribution of encapsulated iron at various inlet spray-drying gas temperatures ($p < 0.05$).

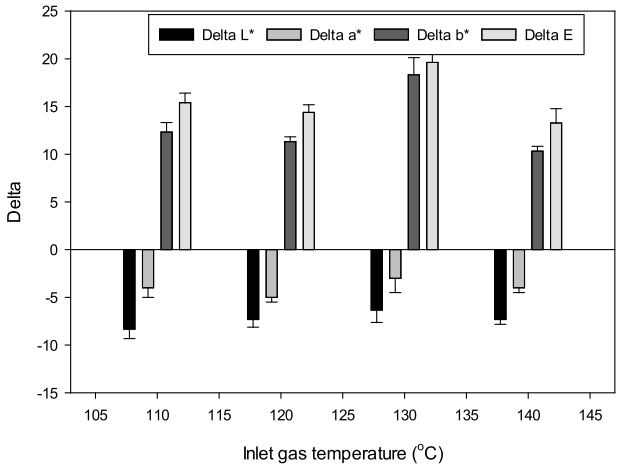

Fig. 3 – Colour evaluation of encapsulated iron at various inlet spray-drying gas temperatures ($p < 0.05$).

The LC results revealed the suitability of hydrolysed glucomannan as a matrix for encapsulating iron. Fig. 1 reveals that the LC in line with inlet temperatures. As the inlet temperature increased from 110 °C to 140 °C, the LC increased from 69.43% to 74.46% ($p < 0.05$). At higher temperatures, a rapid drying rate could be observed in which the water evaporated quickly from the particle, thus leaving behind large hollow particles. Hence, the same amount of sample tended to contain a greater amount of iron at higher temperatures, thus increasing the LC. Similar results have been reported for the encapsulation of mandarin oil at inlet temperatures of 160 °C to 200 °C (Bringas-Lantigua et al., 2011) and the microencapsulation of β-carotene at 110–200 °C (Corrêa-Filho et al., 2019).

3.3. *Solubility and swelling*

The solubility parameter shows the ability of the spray-dried powder to form a solution or suspension in water (Bicudo et al., 2015). Meanwhile, the swelling parameter is a measure of the water content in the network and is typically reported as the ratio of either the mass or the volume of the network in the swollen state to that of the dry state. These parameters were used to evaluate the behaviour of the powders in water. The solubility and swelling of the spray-dried particles are affected by the type and concentration of the matrix, the spray-drying conditions (e.g., inlet gas temperature, feed flow rate and atomisation), and properties of the powder (Tontul and Topuz, 2017). The solubility and swelling of encapsulated iron at various inlet temperatures are presented in Fig. 2. The inlet drying air temperature showed a positive effect on the water solubility and swelling of the powder in the reports by Goula and Adamopoulos (2005), Muzaffar and Kumar (2015), Tran and Nguyen (2018), and Vardin and Yasar (2012). However, in this work, the effects of the inlet temperature on the solubility and swelling were not significant ($p < 0.05$). This result was supported by Shi et al. (2018), who studied the effect of inlet temperature (120–150 °C) on watermelon powder, and by Wong and Tan (2017), who reported the effect of 140–180 °C inlet temperatures on honey jackfruit powder. In these studies, higher inlet temperatures resulted in more hollow space which allowed the solvent to penetrate the particle. A similar phenomenon applied to swelling. The use of higher inlet drying air temperatures produced larger particles, which can be associated with increased swelling (Ferrari et al., 2012; Phisut, 2012). Pajareon and Theerakulkait (2017) suggested that solubility and swelling were due to the engagement of hydroxyl groups that form hydrogen and covalent bonds between the matrix.

3.4. *Particle size distribution*

The particle size distribution is an important physical parameter that had an impact on the handling, stability and storage properties of the particles. Determinations of particle size distribution using the particle size analyser from Malvern Panalytical are presented in Fig. 2. Our findings revealed that the temperature of 140 °C led to the highest average particle size, whereas the temperature of 110 °C led to the lowest average particle size. The average particle size of the 140 °C sample was almost twice as large as that of the particles prepared with the lowest inlet air temperature (110 °C) ($p < 0.05$). Increasing the inlet drying air temperature often resulted in the rapid formation of a crust layer on the droplet surface, making it more difficult for moisture to diffuse out through the particle surface. As a consequence, the particle size was bigger. On the other hand, when the inlet air temperature is lower, the particle remains wet and requires a longer period of time to shrink, thus decreasing its size (Ferrari et al., 2012). In addition to inlet drying air temperature, the particle size distribution is also affected by many other factors, including carrier concentration, carrier type, feed flowrate and atomisation (Tontul and Topuz, 2017). Similar results have been reported in prior studies (Chegini and Ghobadian, 2005; Ferrari et al., 2012; Jumah et al., 2000; Tonon et al., 2011).

3.5. *Colour*

Colour is another important parameter in determining the quality of spray-dried products. Proper colour helps to ensure an attractive appearance for a product. The colour properties of spray-dried products are affected by the natural feed and matrix/carrier material colour, as well as the concentration and the tendency of the matrix to undergo nonenzymatic browning reactions due to the high drying temperatures (Tontul and Topuz, 2017). The colour determination from this study is presented in Fig. 3. The study outcomes indicate that, when in contact with higher drying air temperatures during the spray-drying process, the glucomannan matrix gives negative values for both ΔL^* and Δa^*, whereas Δb^* has a positive value. This means that the product tends to have a darker colour as compared with the native glucomannan pow-

der, which has colour properties of $L_0^* = 68.33$, $a_0^* = 19$, and $b_0^* = 30.67$ ($p < 0.05$). This indicates that a browning reaction occurs during the spray-drying process, making the colour of the powder browner and darker. There was no amino acid content in the encapsulant since 100% glucomannan was used as a matrix. Hence, the browning in this high-temperature process was due to caramelisation, a carbohydrate reaction pathway that can occur either in dry or concentrated solutions when exposed to high temperatures without involving amino acids (Woo et al., 2015). An insignificant effect of the inlet gas temperature on the final colour was observed in this work. Quintas et al. (2007) reported on the colour development of the caramelisation reaction for temperatures of 100–160 °C. Our results demonstrate that having a greater difference between the inlet and outlet temperatures at high temperature ranges has a greater effect on the browning of the encapsulation powders, resulting in more severe changes to the colour of the sample (ΔE). Quintas et al. (2007) reported the processing temperature did not contribute to the lightness of the final product or the final colour difference from the initial solution.

3.6. *Particle morphology*

Fig. 4 shows that different gas inlet temperatures produced various particle sizes and shapes. An irregular particle form characterised by a basin was observed on the particle surface. This irregular shape could be due to water evaporation during the drying process, which left a hollow area inside the droplet, causing shrinkage and the loss of sphericity (Arpagaus et al., 2017). At a magnification of 10,000×, a smooth particle surface was observed. Higher temperatures tended to produce larger round particles. This suggests that higher temperature drying resulted in crust formation on the particle surfaces. In general, higher gas temperatures increase the drying rate, leading to the formation of hollow particles, while lower gas temperatures allow for the creation of more compact particles (Nandiyanto and Okuyama, 2011). The particle shape is affected by both the feed properties (e.g., material type, solid concentration, solvent and surfactant) and the drying conditions (e.g., gas temperature) (Arpagaus et al., 2017). Thus, to produce a solid, round particle for iron encapsulation using glucomannan as the matrix, the concentration of the matrix, active compound and solvent should be altered or a stabiliser should be added so that the particle does not shrink easily.

In this research, scanning electron microscopy–energy-dispersive X-ray (SEM-EDX) spectroscopy was used to confirm the amount of iron on the particles' surfaces. Fig. 5 shows that the native glucomannan powder itself contains iron but at a lower percentage than the encapsulation powder. An increase in the drying air temperature led to an increase in the amount of iron on the surface. Samples made with higher air temperatures had larger particle sizes, which allows for the encapsulation of more iron in the particle, either inside or on the surface of the particle. This result supports the EE determination, wherein increasing the temperature caused a rise in EE.

3.7. *Functional groups*

Fourier-transform infrared spectroscopy analysis was used to elucidate the functional particle groups based on the change in the inlet drying air temperature. The IR spectra of all iron encapsulation samples between 4000 to 400 cm^{-1} were compared with those of native glucomannan and $FeSO_4{\cdot}7H_2O$,

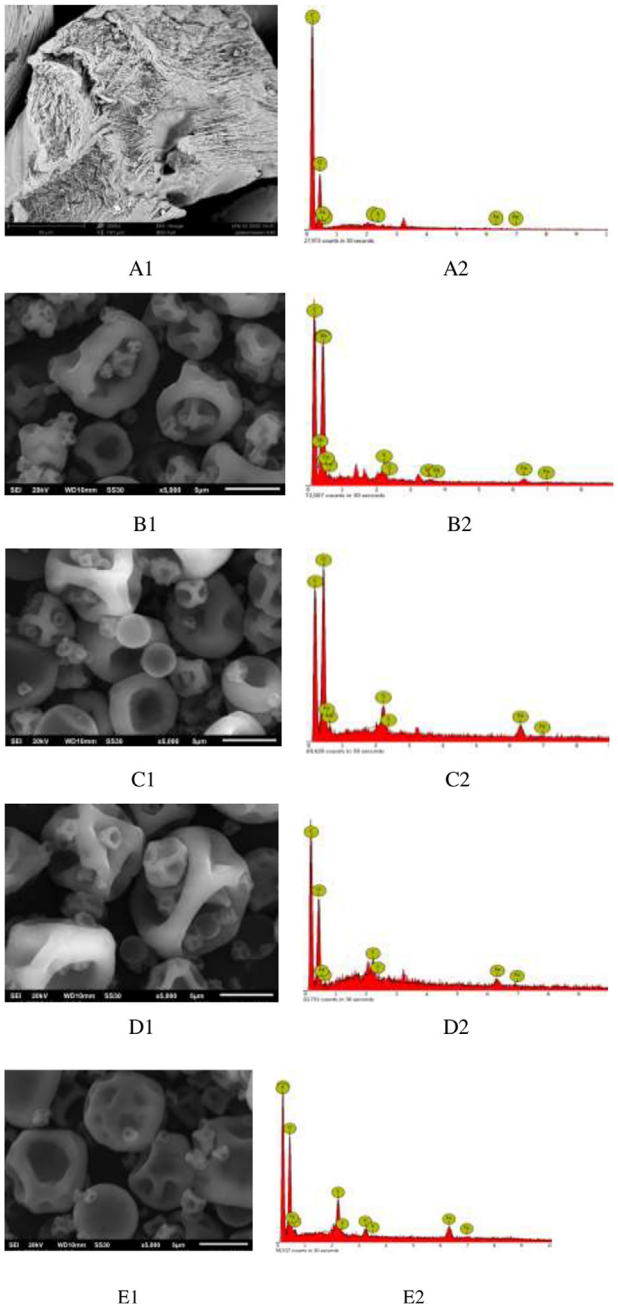

Fig. 4 – SEM images (left) and SEM-EDX spot analyses (right) of native glucomannan powder at 2500× magnification (A) and encapsulated iron powder at 5000× magnification formed at inlet gas temperatures of 110 °C (B), 120 °C (C), 130 °C (D) and 140 °C (E).

the source of the iron (Fig. 6). A wide peak from the O—H group at 3000–3700 cm^{-1} (Wardhani et al., 2019b) was observed in glucomannan, the iron reagent and all of the encapsulation samples. However, methyl and carbonyl groups, which were assigned to the–CH stretch vibration (~2900 cm^{-1}) and the acetyl groups (1720 cm^{-1}), respectively (Liu et al., 2015), were only observed in glucomannan and the encapsulated samples. Ultimately, the results of this study indicate that changes in the gas temperature did not affect the functional groups. The spectrum of iron was similar to that found in the study of Asghari-Varzaneh et al. (2017), which detected the emergence of an iron peak at 620 cm^{-1} in the spectra of the iron-glucomannan particles. A peak from a sulphur compound was found at 1300–1000 cm^{-1} when measuring the iron

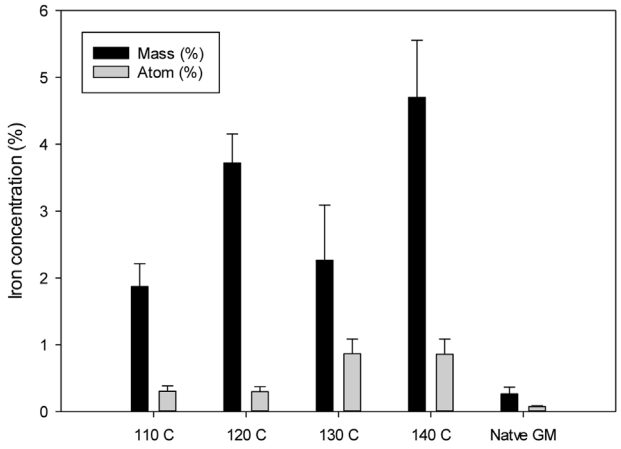

Fig. 5 – Mass and atomic percentages obtained using JEOL JSM-6510 LV of iron encapsulated in particles formed with various inlet gas temperatures in spray-drying.

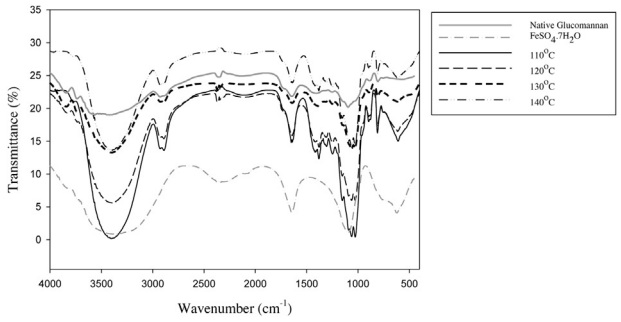

Fig. 6 – IR-spectra of encapsulated iron in various inlet gas temperatures of spray-drying using PerkinElmer-Frontier FT-IR.

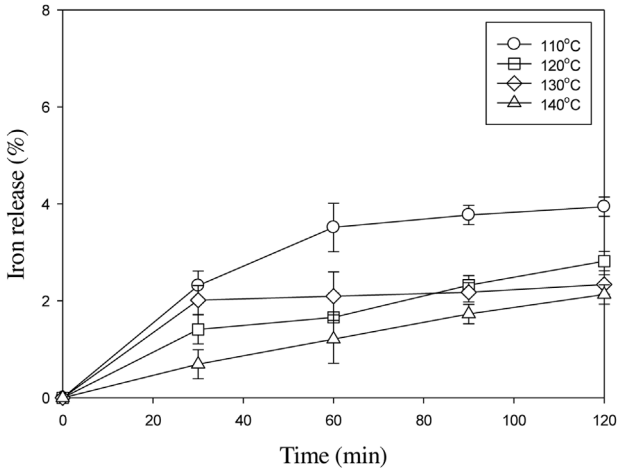

Fig. 7 – Iron released from encapsulation in a phosphate buffer solution at pH 6.8.

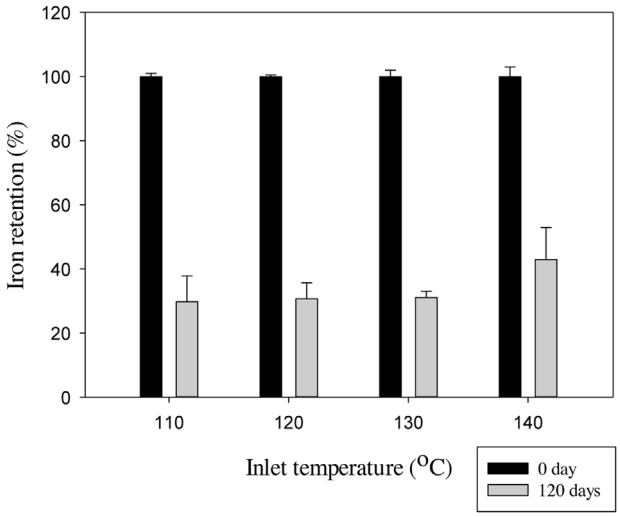

Fig. 8 – Iron stabilisation in a hydrolysed glucomannan encapsulant as a matrix preventing iron oxidation.

compound. The addition of $FeSO_4{\cdot}7H_2O$ as the iron source also allowed the peak around 3400 cm^{-1} to be identified as belonging to O—H groups and the peak at 1100 cm^{-1} to be identified as belonging to a sulphate group (Gaihre et al., 2008; Gotić and Musić, 2007).

3.8. *Release of iron*

The iron release conducted at pH 6.8 in a phosphate buffer was used to represent the release of iron from the matrix, as can be found during food preparation and swallowing. Moreover, neutral pH also represents human saliva, which can vary from pH 5.9–7.9 (Singh et al., 2018). The release of iron at this pH shows the potential to disturb the sense of taste in the mouth. Fig. 7 shows that the lowest inlet temperature released the highest iron concentration ($p < 0.05$). The high release could be due to the formation of a crust shell on the particle surface, as explained in Section 3.1, which retards iron diffusion into the surface powder. This work showed that the maximum iron release in 120 min was 4%. This value was lower than that of Singh et al. (2018), who reported that the iron release in the same period was 10–18% and 12–25% using chitosan and Eudragit, respectively. This result suggests that hydrolysed glucomannan has better potency as iron encapsulant when using the spray-drying method compared to chitosan and Eudragit in protecting iron release.

3.9. *Iron stabilisation*

The efficacy of the hydrolysed glucomannan encapsulant in protecting iron from oxidation was observed at room temperature. As shown in Fig. 8, the iron retention decreased after 120 days of storage. The encapsulation in this work resulted in a matrix type in which the iron was dispersed over the encapsulant powder, including on its surface. During storage, the iron on the surface was in contact with and exposed to air. The diffusion of air into the particle could promote iron degradation. A higher inlet temperature in the spray-drying process lowers the iron degradation rate in the iron-glucomannan powder. The hard crust that formed on the surface of the particles hindered air diffusion (León-Martínez et al., 2010), thus protecting the iron from oxidation.

4. Conclusions

Inlet drying air temperature has a significant effect on LC, particle size, and colour but less impact on moisture content, solubility and swelling. Higher inlet drying air temperatures produce a rounder shape powder, whereas lower temperatures produce irregular shapes that tend to form deep concave surface. Increasingly high temperatures lead to the encapsulation

of more iron on particle surfaces. All samples showed similar functional groups of the particles but at different intensities. The amount of iron release at pH 6.8 was higher for sample of lower inlet temperature. Meanwhile, sample of the highest inlet temperature showed the highest performance in protecting iron from oxidation. Considering the performances, it is recommended that the inlet air temperature for iron spray-drying encapsulation using hydrolysed glucomannan is 130 °C.

Conflict of interest

None declared.

Acknowledgements

This research was funded by the Directorate of Research and Community Service, Directorate General of Higher Education, Ministry of Research, Technology and Higher Education of the Republic of Indonesia through Scheme of *Penelitian Dasar*-2019 (Grant number: 257-29/UN7.P4.3/PP/2019).

References

AOAC, 2020. Official Methods of Analysis, 17th ed. The Association of Official Analytical Chemists, Gaithersburg, MD, USA.

Arpagaus, C., John, P., Collenberg, A., Rütti, D., 2017. Nanocapsules formation by nano spray drying. Nanoencaps. Technol. Food Nutraceut. Ind., 346–401, http://dx.doi.org/10.1016/B978-0-12-809436-5.00010-0.

Asghari-Varzaneh, E., Shahedi, M., Shekarchizadeh, H., 2017. Iron microencapsulation in gum tragacanth using solvent evaporation method. Int. J. Biol Macromol. 103, 640–647, http://dx.doi.org/10.1016/j.ijbiomac.2017.05.047.

Avila, L.E., Cortes Rodríguez, M., Velásquez, C., José, H., 2015. Influence of maltodextrin and spray drying process conditions on sugarcane juice powder quality. Rev. Fac. Nac. Agron. Medellín. 68 (1), 7509–7520, http://dx.doi.org/10.15446/rfnam.v68n1.47839.

Bicudo, M.O.P., Jó, J., Oliveira, G.A.D., Chaimsohn, F.P., Sierakowski, M.R., Freitas, R.A.D., Ribani, R.H., 2015. Microencapsulation of juçara (*Euterpe edulis* M.) pulp by spray drying using different carriers and drying temperatures. Drying Technol. 33 (2), 153–161, http://dx.doi.org/10.1080/07373937.2014.937872.

Bringas-Lantigua, M., Expósito-Molina, I., Reineccius, G.A., López-Hernández, O., Pino, J.A., 2011. Influence of spray-dryer air temperatures on encapsulated mandarin oil. Drying Technol. 29 (5), 520–526, http://dx.doi.org/10.1080/07373937.2010.513780.

Bryszewska, M.A., 2019. Comparison study of iron bioaccessibility from dietary supplements and microencapsulated preparations. Nutrients. 11 (2), 273, http://dx.doi.org/10.3390/nu11020273.

Chegini, G.R., Ghobadian, B., 2005. Effect of spray-drying conditions on physical properties of orange juice powder. Drying Technol. 23 (3), 657–668, http://dx.doi.org/10.1081/DRT-200054161.

Churio, O., Valenzuela, C., 2018. Development and characterization of maltodextrin microparticles to encapsulate heme and non-heme iron. LWT-Food Sci Technol. 96, 568–575, http://dx.doi.org/10.1016/j.lwt.2018.05.072.

Corrêa-Filho, L.C., Lourenço, M.M., Moldão-Martins, M., Alves, V.D., 2019. Microencapsulation of β-carotene by spray drying: effect of wall material concentration and drying inlet temperature. Int. J. Food Sci., 1–12, http://dx.doi.org/10.1155/2019/8914852.

Dantas, D., Pasquali, M.A., Cavalcanti-Mata, M., Duarte, M.E., Lisboa, H.M., 2018. Influence of spray drying conditions on the properties of avocado powder drink. Food Chem. 266, 284–291, http://dx.doi.org/10.1016/j.foodchem.2018.06.016.

Ferrari, C.C., Germer, S.P.M., de Aguirre, J.M., 2012. Effects of spray-drying conditions on the physicochemical properties of blackberry powder. Drying Technol. 30 (2), 154–163, http://dx.doi.org/10.1080/07373937.2011.628429.

Gaihre, B., Aryal, S., Barakat, N.A., Kim, H.Y., 2008. Gelatin stabilized iron oxide nanoparticles as a three dimensional template for the hydroxyapatite crystal nucleation and growth. Mater. Sci. Eng. C 28 (8), 1297–1303, http://dx.doi.org/10.1016/j.msec.2008.01.001.

Gotić, M., Musić, S., 2007. Mćssbauer, FT-IR and FE SEM investigation of iron oxides precipitated from FeSO4 solutions. J. Mol Struct. 834, 445–453, http://dx.doi.org/10.1016/j.molstruc.2006.10.059.

Goula, A.M., Adamopoulos, K.G., 2005. Spray drying of tomato pulp in dehumidified air: II. The effect on powder properties. J. Food Eng. 66 (1), 35–42, http://dx.doi.org/10.1016/j.jfoodeng.2004.02.031.

Guerreiro, F., Pontes, J.F., da Costa, A.M.R., Grenha, A., 2019. Spray-drying of konjac glucomannan to produce microparticles for an application as antitubercular drug carriers. Powder Technol. 342, 246–252, http://dx.doi.org/10.1016/j.powtec.2018.09.068.

Gupta, D.C., 2014. Role of iron (Fe) in body. IOSR J. Appl. Chem. 7 (11), 38–46, e-ISSN: 2278-5736.

Hunt, J.R., 2003. Bioavailability of iron, zinc, and other trace minerals from vegetarian diets. Am. J. Clin. Nutr. 78 (3), 633S–639S, http://dx.doi.org/10.1093/ajcn/78.3.633S.

Jana, S., Gandhi, A., Jana, S., 2017. Nanotechnology in bioactive food ingredients: its pharmaceutical and biomedical approaches. Nanotechnol. Appl. Food., 21–41, http://dx.doi.org/10.1016/B978-0-12-811942-6.00002-9.

Jiang, M., Li, H., Shi, J., Xu, Z., 2018. Depolymerized konjac glucomannan: preparation and application in health care. J. Zhejiang Univ. Sci. B (7), 505–514, http://dx.doi.org/10.1631/jzus.B1700310.

Jumah, R.Y., Tashtoush, B., Shaker, R.R., Zraiy, A.F., 2000. Manufacturing parameters and quality characteristics of spray dried jameed. Drying Technol. 18 (4–5), 967–984, http://dx.doi.org/10.1080/07373930008917747.

Liu, J., Xu, Q., Zhang, J., Zhou, X., Lyu, F., Zhao, P., Ding, Y., 2015. Preparation, composition analysis and antioxidant activities of konjac oligo-glucomannan. Carbohydr. Polym. 130, 398–404, http://dx.doi.org/10.1016/j.carbpol.2015.05.025.

Mishra, P., Mishra, S., Mahanta, C.L., 2014. Effect of maltodextrin concentration and inlet temperature during spray drying on physicochemical and antioxidant properties of amla (*Emblica officinalis*) juice powder. Food Bioprod. Process. 92 (3), 252–258, http://dx.doi.org/10.1016/j.fbp.2013.08.003.

Moghaddam, A.D., Pero, M., Askari, G.R., 2017. Optimizing spray drying conditions of sour cherry juice based on physicochemical properties, using response surface methodology (RSM). J. Food Sci. Technol. 54 (1), 174–184, http://dx.doi.org/10.1007/s13197-016-2449-8.

Muzaffar, K., Kumar, P., 2015. Parameter optimization for spray drying of tamarind pulp using response surface methodology. Powder Technol. 279, 179–184, http://dx.doi.org/10.1016/j.powtec.2015.04.010.

Nandiyanto, A.B.D., Okuyama, K., 2011. Progress in developing spray-drying methods for the production of controlled morphology particles: from the nanometer to submicrometer size ranges. Adv. Powder Technol. 22 (1), 1–19, http://dx.doi.org/10.1016/j.apt.2010.09.011.

Nedovic, V., Kalusevic, A., Manojlovic, V., Levic, S., Bugarski, B., 2011. An overview of encapsulation technologies for food applications. Proc. Food Sci. 1, 1806–1815, http://dx.doi.org/10.1016/j.profoo.2011.09.265.

Pajareon, S., Theerakulkait, C., 2017. Effects of spray drying at different inlet air temperatures on antioxidative activity and some properties of Homnil rice bran extract powder. Pakistan J. Nutr. 16, 782–788.

Phisut, N., 2012. Spray drying technique of fruit juice powder: some factors influencing the properties of product. Int. Food Res. J. 19 (4), 1297–1306.
Quintas, M., Teresa, R.S., Brandão, T.R.S., Silva, C.L.M., 2007. Modeling colour changes during the caramelization reaction. J. Food Eng. 83 (4), 483–491, http://dx.doi.org/10.1016/j.jfoodeng.2007.03.036.
Rigon, R.T., Noreña, C.P.Z., 2016. Microencapsulation by spray-drying of bioactive compounds extracted from blackberry (*rubus fruticosus*). J. Food Sci. Technol. 53 (3), 1515–1524, http://dx.doi.org/10.1007/s13197-015-2111-x.
Romita, D., Cheng, Y.L., Diosady, L.L., 2011. Microencapsulation of ferrous fumarate for the production of salt double fortified with iron and iodine. Int. J. Food Eng. 7 (3), http://dx.doi.org/10.2202/1556-3758.2122.
Santhalakshmy, S., Bosco, S.J.D., Francis, S., Sabeena, M., 2015. Effect of inlet temperature on physicochemical properties of spray-dried jamun fruit juice powder. Powder Technol. 274, 37–43, http://dx.doi.org/10.1016/j.powtec.2015.01.016.
Shi, Y., Wang, J., Wang, Y., Zhang, H., Ma, Y., Zhao, X., Zhang, C., 2018. Inlet temperature affects spray drying quality of watermelon powder. Czech J. Food Sci. 36 (4), 321–328, http://dx.doi.org/10.17221/406/2017-CJFS.
Singh, A.P., Siddiqui, J., Diosady, L.L., 2018. Characterizing the pH-dependent release kinetics of food-grade spray drying encapsulated iron microcapsules for food fortification. Food Bioprocess Technol. 11, 435–446, http://dx.doi.org/10.1007/s11947-017-2022-0.
Sosnik, A., Seremeta, K.P., 2015. Advantages and challenges of the spray-drying technology for the production of pure drug particles and drug-loaded polymeric carriers. Adv. Colloid Interface Sci. 223, 40–54, http://dx.doi.org/10.1016/j.cis.2015.05.003.
Tonon, R.V., Freitas, S.S., Hubinger, M.D., 2011. Spray drying of açai (*Euterpe oleraceae* Mart.) juice: effect of inlet air temperature and type of carrier agent. J. Food Process. Preserv. 35 (5), 691–700, http://dx.doi.org/10.1111/j.1745-4549.2011.00518.x.
Tontul, I., Topuz, A., 2017. Spray-drying of fruit and vegetable juices: effect of drying conditions on the product yield and physical properties. Trends Food Sci. Technol. 63, 91–102, http://dx.doi.org/10.1016/j.tifs.2017.03.009.
Tran, T.T.A., Nguyen, H.V.H., 2018. Effects of spray-drying temperatures and carriers on physical and antioxidant properties of lemongrass leaf extract powder. Beverages. 4 (4), 84, http://dx.doi.org/10.3390/beverages4040084.
Vardin, H., Yasar, M., 2012. Optimisation of pomegranate (*Punica Granatum* L.) juice spray-drying as affected by temperature and maltodextrin content. Int. J. Food Sci. Technol. 47 (1), 167–176, http://dx.doi.org/10.1111/j.1365-2621.2011.02823.x.
Veerabhadraswamy, M., Devaraj, T.D., Jayanna, B.K., 2018. Second derivative spectrophotometric determination of iron(II) and ruthenium(III) using 1, 10-phenanthroline. Anal. Chem. Lett. 8 (6), 757–768, http://dx.doi.org/10.1080/22297928.2018.1548944.
Wardhani, D.H., Nugroho, F., Muslihuddin, M., 2015. Extraction of glucomannan of porang tuber (*Amorphophallus onchophillus*) by using IPA. AIP Conference Proceedings, 1699, 1, 060007, http://dx.doi.org/10.1063/1.4938361.
Wardhani, D.H., Aryanti, N., Etnanta, F.N., Ulya, H.N., 2019a. Modification of glucomannan of *Amorphophallus oncophyllus* as an excipient for iron encapsulation performed using the gelation method. Acta Sci. Polonorum Technol. Aliment. 18 (2), 173–184, http://dx.doi.org/10.17306/J.AFS. 2019.0651.
Wardhani, D.H., Vázquez, J.A., Ramdani, D.A., Lutfiati, A., Aryanti, N., Cahyono, H., 2019b. Enzymatic purification of glucomannan from *Amorphophallus oncophyllus* using α-amylase. Biosci. J. 35 (1), 277–288, http://dx.doi.org/10.14393/BJ-v35n1a2019-41766.
Wattanaprasert, S., Borompichaichartkul, C., Vaithanomsat, P., Srzednicki, G., 2017. Konjac glucomannan hydrolysate: a potential natural coating material for bioactive compounds in spray drying encapsulation. Eng. Life Sci. 17 (2), 145–152, http://dx.doi.org/10.1002/elsc.201600016.
WHO, 2001. Iron deficiency anemia. assessment, prevention, and control. In: A Guide for Programme Managers, 47-62. WHO/NHD/01.3.
Wong, C.W., Tan, H.H., 2017. Production of spray-dried honey jackfruit (*Artocarpus heterophyllus*) powder from enzymatic liquefied puree. J. Food Sci. Technol. 54 (2), 564–571.
Woo, K.S., Kim, H.Y., Hwang, I.G., Lee, S.H., Jeong, H.S., 2015. Characteristics of the thermal degradation of glucose and maltose solutions. Prev. Nutr. Food Sci. 20 (2), 102–109, http://dx.doi.org/10.3746/pnf.2015.20.2.102.